Journal of Solid State Chemistry 182 (2009) 1506–1514

Contents lists available at ScienceDirect

Journal of Solid State Chemistry

journal homepage: www.elsevier.com/locate/jssc

$Cr_xRe_{1-x}O_2$ oxides with different rutile-like structures: changes in the electronic configuration and resulting physical properties

D. Mikhailova [a,b,*], H. Ehrenberg [a,b], D. Trots [a,c], G. Brey [d], S. Oswald [b], H. Fuess [a]

[a] Institute for Materials Science, Darmstadt University of Technology, Petersenstr. 23, D-64287 Darmstadt, Germany
[b] Institute for Complex Materials, IFW Dresden, Helmholtzstr. 20, D-01069 Dresden, Germany
[c] Hamburger Synchrotronstrahlungslabor, Notkestr. 85, D-22603 Hamburg, Germany
[d] Institute for Geosciences, Johann Wolfgang Goethe-University Frankfurt am Main, Altenhöferallee 1, D-60438 Frankfurt am Main, Germany

ARTICLE INFO

Article history:
Received 29 November 2008
Received in revised form
23 March 2009
Accepted 29 March 2009
Available online 8 April 2009

PACS:
61.66.Fn

Keywords:
Chromium rhenium oxides $Cr_xR_{1-x}O_2$
Rutile-like structures
Anisotropic thermal expansion
Re–Re metallic bond

ABSTRACT

Mixed chromium–rhenium oxides, $Cr_xRe_{1-x}O_2$ with $0.31 \leqslant x \leqslant 0.66$, have been synthesized for the first time by high-pressure high-temperature synthesis and in evacuated quartz tubes. The crystal structures of the compounds have been determined by single crystal and powder X-ray diffraction. Depending on synthesis conditions (pressure and temperature) these phases crystallize either in a tetragonal structure ($P4_2/mnm$) with statistical distribution of metal ions on one site (rutile-type), with cation ordering along *c*-axis (trirutile-type), or in a monoclinic rutile-like structure ($C2/m$) with ordering of Cr- and Re-cations and metallic Re–Re bonds. The "*a*" parameter of the tetragonal unit cell increases with increasing Re content whereas the "*c*" parameter decreases, indicating a strengthening of the Re–Re bond. The thermal stability of tetragonal $Cr_xRe_{1-x}O_2$ in Ar-atmosphere depends on the Re-content, decomposition is observed at 1241 K for $x = 0.34$, but already at 966 K for $x = 0.5$. The thermal expansion of $Cr_xRe_{1-x}O_2$ is anisotropic with a larger expansion coefficient in the "*c*" direction. Tetragonal $Cr_xRe_{1-x}O_2$ with $0.31 \leqslant x < 0.54$ order antiferromagnetically at low temperatures with T_N depending on the Cr-content *x*.

1. Introduction

A rutile-type structure is adopted by a lot of complex oxides ABO_4, A_2BO_6 or $AA'BO_6$, when all cations have a charge higher or equal to +2 and octahedral coordination is preferred. Cation sites can be occupied statistically by different elements if their ionic charges and sizes do not differ significantly. Otherwise, superstructures with cation order are formed [1]. The transition metals that form oxides with rutile structure have an incompletely filled *d* shell, which is responsible for the variety of properties of these compounds.

Several complex oxides of Cr^{3+} with rutile, trirutile or rutile-like structure exist, because the ionic radius of Cr^{3+} (0.62 Å) is close to the one of Ti^{4+} (0.61 Å) for octahedral oxygen coordination [1–3]. The rutile-type structure with a statistical distribution of cations is known, for example, for $CrMO_4$ (M = Sb, Nb, Ta) [1]. Recently a solid solution of $CrV_{1-x}Sb_xO_4$ ($x = 0$–1) with rutile-type structure has been synthesized [4]. Depending on the Cr/*M* ratio in $Cr_xM_{1-x}O_2$ systems, different rutile-structure derivatives can be formed. For instance, compounds containing Cr(III) and heavy six-valence elements with the composition Cr_2MO_6 (M = Te [5], Mo, W [6–8]) often crystallize in the ordered trirutile structure ($P4_2/mnm$), whereas $CrMO_4$ (M = Mo [9], W [10]) has a monoclinic distorted rutile-like structure with M^{+5} stabilized by the formation of *M*–*M* pairs with metallic bonds. In the system $Cr_xMo_{1-x}O_2$ four different rutile-related phases were found: a monoclinic MoO_2-type for $0 < x < 0.12$, a solid solution with a tetragonal rutile-structure for $0.12 < x < 0.36$ [11,12], a monoclinic distorted rutile for $0.36 < x < 0.5$ ($CrMoO_4$-type), and a trirutile structure for $x = 0.667$ [8]. Magnetic properties of Cr-containing compounds with rutile-like structure depend strongly on the composition: for instance, Cr_2WO_6 and Cr_2TeO_6 are antiferromagnetically ordered at 4.2 K with a magnetic unit cell identical with the crystallographic cell and with small values for the ordered magnetic moments of the Cr^{3+} ions (2.14μ_B and 2.45μ_B, respectively) [7] compared to a typical value of 2.80μ_B for Cr^{3+} ion. The mixed dioxides $Cr_xMo_{1-x}O_2$ in the range of $0.0 < x < 0.5$ demonstrate ferrimagnetic behavior with Curie temperatures below 200 K. The experimental effective magnetic moment of $Cr_xMo_{1-x}O_2$ ($0.0 < x < 0.5$) in the paramagnetic region is in good agreement with the calculated spin-only values of Cr^{3+} and indicates no significant contribution from the Mo ions. $CrMoO_4$ is antiferromagnetic with a Néel temperature of 100 K, similar to

* Corresponding author at: Institute for Materials Science, Darmstadt University of Technology, Petersenstr. 23, D-64287 Darmstadt, Germany.
Fax: +49 6151 166023.
E-mail address: d.mikhailova@ifw-dresden.de (D. Mikhailova).

0022-4596/$ - see front matter © 2009 Elsevier Inc. All rights reserved.
doi:10.1016/j.jssc.2009.03.025

isostructural $CrWO_4$ [12], which has an antiferro-paramagnetic transition between 40 and 45 K.

Ternary oxides in the system Cr–Re–O are less intensively investigated, although these systems offer an additional degree of freedom due to the ability of the Re ion to adopt formal oxidation states between +4 and +7 in complex oxides with different resulting properties. Both end members, CrO_2 [13] and the monoclinic modification of ReO_2 [14], have a rutile-like structure. A new modification of ReO_2 with rutile structure was also recently reported [15]. Sleight [16] has reported on Cr_2ReO_6, prepared under high-pressure high-temperature conditions, and proposed for this compound a trirutile structure. This suggestion was based on the similarities of the cell metric and diffraction patterns with analogous tungsten compounds, but neither a structure refinement was performed, nor physical properties were investigated. In this work we report on the preparation of $Cr_xRe_{1-x}O_2$ compounds with different compositions by two different methods: a high-pressure high-temperature synthesis or in sealed silica tubes. The crystal structures have been determined by single crystal and powder diffraction. Thermal behavior and magnetic properties have also been investigated and are discussed with respect to their dependence on composition.

2. Experimental

High-pressure high-temperature synthesis (*HPHT*). High-pressure high-temperature syntheses of $Cr_xRe_{1-x}O_2$ were performed in a Girdle-Belt apparatus up to 5 GPa and in a multianvil press for pressures up to 9 GPa. For the Girdle-Belt apparatus, a graphite furnace with a platinum capsule inside containing the reactants and pyrophyllite as the pressure-transmitting medium were used. Pressure transmission for the multianvil press was realized by MgO-octahedra, hexagonal BN was used as crucible material. A small amount of $CrBO_3$ was detected as impurity on the sample surface after the synthesis, but could easily be removed from the main product.

Mixtures of Cr_2O_3 (Strem Chemicals, 99.999%) and ReO_3 (Strem Chemicals, 99.9%) or of Cr_2O_3, ReO_3 and Re (Strem Chemicals, 99.99%) were taken as starting materials. The sample holder was pressed up to the required pressure, before temperature was raised to 1473–1673 K with a rate of 50 K/min. The heating current was switched off after 60–120 min, and pressure was released after cooling to room temperature.

Synthesis in sealed silica tubes. To obtain $Cr_xRe_{1-x}O_2$ ($0.31 \leqslant x \leqslant 0.44$), chromium perrhenate hydrate $Cr(ReO_4)_3 \cdot 6H_2O$ [17] was used as a precursor. It was synthesized from freshly prepared chromium oxide Cr_2O_3, obtained from the aqueous solution of $CrCl_3$ ($CrCl_3 \cdot 6H_2O$, Aldrich, p.a.) with $NH_3 \cdot aq$ (Aldrich, p.a.) as precipitating agent followed by an annealing of the precipitate at 673 K during 2 h in air, and $HReO_4$, obtained from Re powder (Stream, 99.99%) and a 30% solution of H_2O_2 (Aldrich, p.a.) by a standard method described elsewhere [18]. The powder of chromium perrhenate hydrate was dried in a drying chamber and in a quartz crucible placed into a silica tube, which was held in dynamic vacuum at 743–803 K during 2–4 h. After that the tube was sealed and annealed at 873–1423 K during 20–40 h. Chromium perrhenate hydrate decomposes in dynamic vacuum at elevated temperature with elimination of gaseous Re_2O_7 and O_2. The Cr:Re ratio in the solid reaction product is therefore dependent on the details of synthesis conditions such as temperature, annealing time, mass of the perrhenate and free silica tube volume, so that different compositions $Cr_xRe_{1-x}O_2$ could be obtained by a variation of these parameters.

X-ray powder diffraction (*XPD*). Phase analysis and structure refinement were performed based on X-ray powder diffraction with a STOE STADI P diffractometer (Mo$K\alpha_1$-radiation, $\lambda = 0.7093$ Å) in steps of 0.02° for 2θ from 3° to 45° in flat–sample transmission mode.

X-ray synchrotron diffraction. High-temperature structure investigations of $Cr_{0.50}Re_{0.50}O_2$ and $Cr_{0.33}Re_{0.67}O_2$ powders in the temperature range of 295–1173 K have been performed by synchrotron diffraction at HASYLAB/DESY (Hamburg, Germany) at beam-line B2 [23] in Debye-Scherrer mode using the on-site readable image-plate detector OBI [24] and a STOE furnace equipped with a EUROTHERM temperature controller and a capillary spinner. Quartz capillaries 0.3 mm were filled with powdered $Cr_xRe_{1-x}O_2$ in a glove-box under Ar-atmosphere, sealed and mounted inside the STOE furnace. Diffraction data were collected in steps of 0.004° from $2\theta = 4°$ to 40° in temperature steps of 100 K. The wavelength of 0.49962(1) Å was selected by a double-crystal monochromator and determined from the positions of eight reflections from a LaB_6 reference material. After heating up to 1173 K the samples were analyzed again at room temperature to check if any irreversible changes can be detected.

All diffraction patterns have been analyzed by using the software package WinPLOTR [19]. For structure determination, a full-profile Rietveld refinement was performed with an isotropic approximation for the thermal displacement parameters, which were refined constrained for Cr and Re atoms, but independently for oxygen atoms.

Single-crystal X-ray diffraction. The crystal structure of $Cr_{1-x}Re_xO_2$ was solved by single-crystal X-ray diffraction using the Xcalibur system from Oxford Diffraction. The software packages SHELXS [20] and SHELXL [21] were used for structure solution and refinement as included in X-STEP32 [22].

Magnetic susceptibility. The magnetic properties of $Cr_xRe_{1-x}O_2$ have been studied with a superconducting quantum interference device (SQUID) from Quantum Design. Measurements were performed upon heating (field-cooling mode) in the temperature range from 1.7 to 350 K and with an applied field strength of 100 G or 500 G.

Differential thermal analysis (*DTA-TG*). A simultaneous thermal analyzer NETZSCH STA 429 operated with dry and purified Ar was used to register mass loss and thermal flux curves. About 30 mg of $Cr_{0.50}Re_{0.50}O_2$ and $Cr_{0.33}Re_{0.67}O_2$ were heated in an Al_2O_3-crucible in Ar-atmosphere with a rate of 5 K/min from 293 up to 1423 K.

Thermogravimetry (*TG*). The Re contents in the $Cr_xRe_{1-x}O_2$ samples were determined by thermogravimetric measurements, based on the ability of Re in numerous complex oxides to be oxidized to volatile Re_2O_7 by heating in air. Samples were carefully weighed in Al_2O_3 crucibles before and after annealing in air at 1223 K during 24 h. The phase composition of the residue (Cr_2O_3) was always checked by X-ray diffraction.

Electron probe microanalysis (*EPMA*). Compositions in individual grains were checked by electron probe microanalysis using a CAMECA Instruments CAMEBAX SX-50 electron microprobe.

Scanning electron microscopy (*SEM*). Morphologies of $Cr_xRe_{1-x}O_2$ samples, prepared in sealed silica tubes and by HPHT synthesis, were observed by scanning electron microscopy (SEM Philips XL-30 FEG operated at 25 kV).

X-ray photoelectron spectroscopy (*XPS*). X-ray photoelectron spectra were measured on a PHI 5600 CI system using an Al$K\alpha$ 350 W monochromatized X-ray source and a hemispherical analyzer at a pass energy of 29 eV. When necessary, surface charging was minimized by means of a low-energy electron flood gun. The system base pressure was about 10^{-9} mbar. ReO_3 (Strem Chemicals, 99.9%) was used as a reference material for the estimation of the valence states of the Re ions in the Cr,Re-containing phases. The binding energy scale was calibrated from carbon contamination using the C1 s peak at 285.0 eV.

3. Results

3.1. Synthesis and characterization of $Cr_xRe_{1-x}O_2$

3.1.1. Synthesis in a silica tube

All samples prepared by the thermal decomposition of $Cr(ReO_4)_3 \cdot 6H_2O$ in vacuum at 743–803 K appeared as a black fine powder. The X-ray diffraction data of the samples annealed at 743 K showed mostly the presence of an amorphous material while the degree of crystallinity increased with temperature and time of annealing. After annealing in evacuated sealed tubes at 873–1273 K during 20 h $Cr_xRe_{1-x}O_2$ samples were finely crystallized, having even-grained particles with a narrow distribution of particle sizes, see Fig. 1(a). By changing the time of annealing of the precursor in dynamic vacuum and the synthesis temperature we prepared almost single phase samples of $Cr_xRe_{1-x}O_2$ with $0.31 \leqslant x \leqslant 0.44$. Samples with a Cr-content $x \geqslant 0.39$ require a lower temperature of synthesis (973–1023 K), otherwise Cr_2O_3 and ReO_2 appeared together with $Cr_xRe_{1-x}O_2$.

All reflections in the diffraction patterns can be explained based on tetragonal unit cells with lattice parameters $a = 4.7$ Å and $c = 2.8$ Å, except two small peaks at 2θ at $\sim 11^\circ$ and 13° for some samples, which belong to the orthorhombic modification of ReO_2 [33] (less than 2.5% w/w). Samples were stable at ambient conditions at least for six months, but decompose into Cr_2O_3 and Re_2O_7 (gas) by heating in air. The Re-contents in the samples, determined by thermogravimetry and by EPMA performed for 5–6 spots on several grains, are in agreement with each other, confirming homogeneity of the product. For example, thermogravimetric data gave a composition of $Cr_{0.32(2)}Re_{0.68(2)}O_2$ and an average amount of 31 at.% Cr and 69 at.% Re by EPMA.

Attempts to grow single crystals from $CrRe_2O_6$ powder in an evacuated sealed silica tube at higher temperature (1423 K) during 34–40 h led to the decomposition of $Cr_xRe_{1-x}O_2$: Cr_2O_3, ReO_2 and ReO_3 were found together with $Cr_xRe_{1-x}O_2$ (50% w/w) by X-ray diffraction, but no single crystals of sufficient size for X-ray structure analysis were found.

3.1.2. High-pressure high-temperature synthesis

$Cr_xRe_{1-x}O_2$ crystals with tetragonal symmetry and compositions $x = 0.54$, 0.50 and 0.34, confirmed by EPMA for various crystallites from each sample, were obtained at 1623 K and 5 GPa (Fig. 1(b)). The educts did not yet react at 3 GPa and 1323 K. Note, that the average crystal size of $Cr_xRe_{1-x}O_2$ was larger for the samples with higher Cr-content. The $Cr_{0.34}Re_{0.66}O_2$ sample contained about 3% (w/w) ReO_2 (ort.), $Cr_{0.50}Re_{0.50}O_2$ was obtained as a single phase, and a small amount of Cr_2O_3 and an unknown phase were detected as impurities in the $Cr_{0.54}Re_{0.46}O_2$ sample. The diffraction pattern of $Cr_{0.50}Re_{0.50}O_2$ is shown in Fig. 2(a) and gives $a = 4.65748(9)$ Å, $c = 2.86697(6)$ Å.

The phase formation in the system Cr–Re–O is rather complicated, depending on composition, synthesis temperature

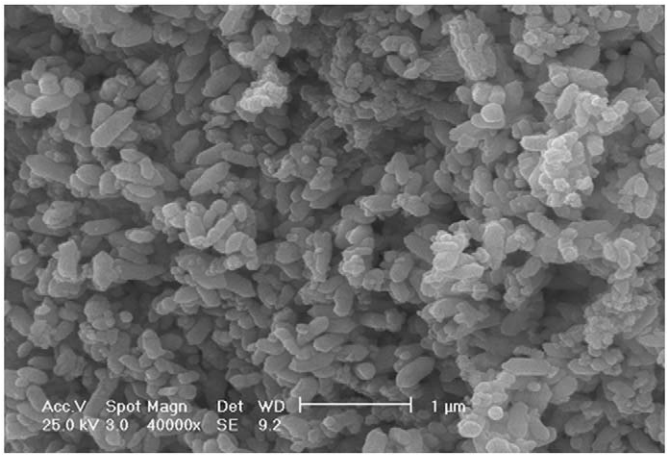

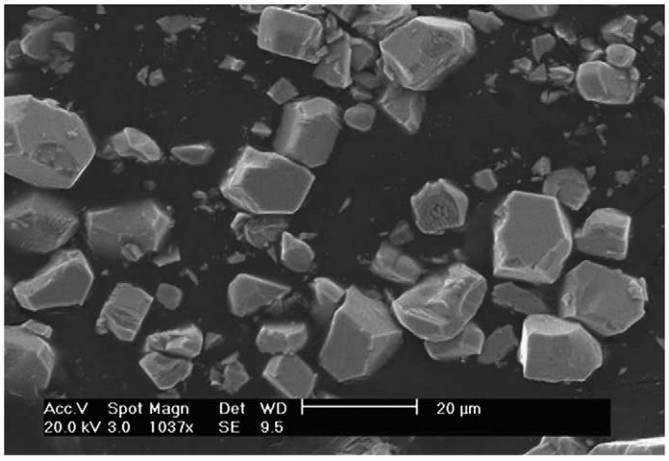

Fig. 1. (a) SEM image of $Cr_xRe_{1-x}O_2$, prepared by decomposition of $Cr(ReO_4)_3 \cdot 6H_2O$ in vacuum followed by annealing in a sealed silica tube at 903 K. (b) SEM image of $Cr_{0.54}Re_{0.46}O_2$, prepared by high-pressure high-temperature synthesis.

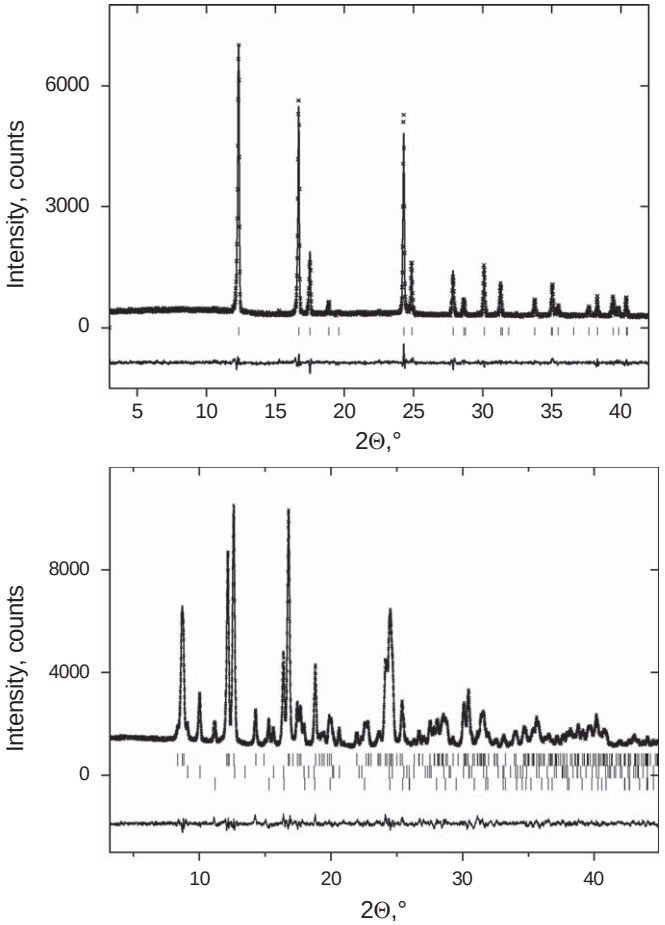

Fig. 2. (a). X-ray diffraction pattern of $Cr_{0.50}Re_{0.50}O_2$ ($P4_2/mnm$) with random cation distribution, observed and calculated profiles together with their difference curve. (b). X-ray diffraction pattern of the sample with overall composition "Cr_2ReO_6", obtained at 8 GPa and 1473 K; observed and calculated profiles together with their difference curve. Tick marks represent from top to bottom the positions of reflections for the monoclinic modification of $Cr_xRe_{1-x}O_2$ ($C2/m$), Cr_2ReO_6 ($P4_2/mnm$) with trirutile-structure and Cr_2O_3.

Table 1
Details of X-ray single-crystal data collection and structure refinement for $Cr_{0.54}Re_{0.46}O_2$, $Cr_{0.50}Re_{0.50}O_2$ and $Cr_{0.34}Re_{0.66}O_2$.

Crystal data			
Chemical formula	$Cr_{0.54}Re_{0.46}O_2$	$Cr_{0.50}Re_{0.50}O_2$	$Cr_{0.34}Re_{0.66}O_2$
Formula weight	143.10	151.10	172.57
Crystal system	Tetragonal	Tetragonal	Tetragonal
Space group	$P4_2/mnm$	$P4_2/mnm$	$P4_2/mnm$
Unit cell dimensions (Å)	$a = 4.609(2)$, $c = 2.914(2)$	$a = 4.671(3)$, $c = 2.861(4)$	$a = 4.689(4)$, $c = 2.836(3)$
Cell volume (Å^3)	61.90(6)	62.42(10)	62.35(10)
Z	2	2	2
Calculated density (g/cm^3)	7.677	8.039	9.191
Radiation type (Å)	Mo$K\alpha$ ($\lambda = 0.71073$)		
No. of reflections for the determination of cell parameters	81	128	171
Temperature (K)	293(2)	293(2)	293(2)
Crystal form, color	Prism, black	Prism, black	Prism, black
Crystal size (mm)	$0.030 \times 0.025 \times 0.020$	$0.038 \times 0.035 \times 0.029$	$0.030 \times 0.025 \times 0.020$
Data collection			
Diffractometer	Oxford diffraction Xcalibur (TM); single-crystal X-ray diffractometer with sapphire CCD detector		
Data collection method	Rotation method data acquisition using ω and φ scans(s)		
Absorption coefficient (mm^{-1})	52.16	55.46	70.57
$F(000)$	127	131	147
θ range for data collection	6.26°–26.72°	6.18°–26.33°	6.15°–30.88°
Range of h, k, l	$-3 \leqslant h \leqslant 5$, $-5 \leqslant k \leqslant 5$, $-2 \leqslant l \leqslant 3$	$-5 \leqslant h \leqslant 3$, $-5 \leqslant k \leqslant 5$, $-2 \leqslant l \leqslant 3$	$-4 \leqslant h \leqslant 5$, $-4 \leqslant k \leqslant 6$, $-3 \leqslant l \leqslant 4$
Reflections collected/unique	175/45 (R(int) = 0.0252)	175/46 (R(int) = 0.0226)	290/66 (R(int) = 0.0288)
Completeness to $\theta = 26.72°$ (%)	97.8	100.0	98.5
Refinement method	Full-matrix least-squares on F^2		
Data/restraints/parameters	45/0/10	46/0/9	66/0/9
Goodness-of-fit on F^2	1.148	1.118	1.081
Final R indices (I>2sigma(I))	$R_1 = 0.0154$, $wR_2 = 0.0372$	$R_1 = 0.0142$, $wR_2 = 0.0302$	$R_1 = 0.0245$, $wR_2 = 0.0579$
R indices (all data)	$R_1 = 0.0260$, $wR_2 = 0.0383$	$R_1 = 0.0200$, $wR_2 = 0.0314$	$R_1 = 0.0277$, $wR_2 = 0.0584$
Extinction coefficient	0.024(8)	0.057(9)	0.13(2)
Largest diff. peak and hole	0.511 and −0.980e Å^{-3}	0.935 and −0.657e Å^{-3}	1.230 and −2.218e Å^{-3}

and pressure. The increase of the synthesis pressure up to 9 GPa in the temperature range of 1473–1673 K led for Cr- or Re-rich compositions to the formation of phases with a partial ordering of cations. For the initial composition "$Cr_{0.67}Re_{0.33}O_2$" a mixture of three phases was detected directly after the synthesis: the monoclinic rutile-like modification of $Cr_xRe_{1-x}O_2$ with metallic Re–Re bonds like in the low-temperature form of $NiRe_2O_6$ [34], Cr_2O_3 and a small amount of orthorhombic ReO_2. Monoclinic $Cr_xRe_{1-x}O_2$ undergoes a structural phase transformation at ambient conditions: after three months, Cr_2ReO_6 with tetragonal trirutile-structure, a smaller amount of the monoclinic modification of $Cr_xRe_{1-x}O_2$ and Cr_2O_3 were found, see Fig. 2(b). "$Cr_{0.33}Re_{0.67}O_2$" does not exist as a single rutile-type phase at 9 GPa and 1473 K, and a mixture of the monoclinic rutile-like modification of $Cr_xRe_{1-x}O_2$ with metallic Re–Re bonds and orthorhombic ReO_2 were detected as reaction products instead. Increasing the pressure yields phases with metallic Re–Re bonds, so that the application of pressure is probably supporting the formation of metallic bonds in general.

3.2. Crystal structures

3.2.1. Crystal structure of $Cr_xRe_{1-x}O_2$ with a random distribution of cations

According to single crystal diffraction data, $Cr_xRe_{1-x}O_2$ phases with $x = 0.31$–0.54 crystallize in a rutile-type structure, space group $P4_2/mnm$, with lattice parameters depending on x (Tables 1–3). In all these compounds Cr and Re ions occupy statistically the cation site ($2a$) of the rutile structure. MO_6 octahedra are slightly distorted: two M–O distances are shorter than the other four (Table 3). The average Cr–O and Re–O distances do not change significantly with x in $Cr_xRe_{1-x}O_2$: 1.957(5) Å for $x = 0.54$, 1.962(4) for $x = 0.50$ and 1.962(5) for $x = 0.34$. These values are similar to Cr–O distances in Cr_2TeO_6 (1.965 Å) and slightly shorter than in Cr_2WO_6 (1.974 Å) with a trirutile-structure type [7]. An average Re–O distance of 1.957–1.962 Å is characteristic for Re^{+5} in octahedral coordination, for example the average Re–O distance in $CoReO_4$ with rutile-like structure is equal to 1.95 Å [25], and the sum of Re^{+5} and O^{2-} ionic radii is also equal to 1.95 Å [3].

It is not possible to determine the Cr/Re–ratios in $Cr_xRe_{1-x}O_2$ precisely from refinements based on single-crystal X-ray diffraction data, because only broad minima of the R_1-values as function of the Cr/Re–ratio on the ($2a$) site exist for all investigated crystals,

Table 2
Atomic coordinates for rutile-type $Cr_xRe_{1-x}O_2$.

Atom	Site	x	y	z	Occup.
$Cr_{0.54}Re_{0.46}O_2$					
Re/Cr	$2a$	0	0	0	0.46/0.54
O	$4f$	0.2982(13)	0.2982(13)	0	1.0
$Cr_{0.50}Re_{0.50}O_2$					
Re/Cr	$2a$	0	0	0	0.50/0.50
O	$4f$	0.2958(7)	0.2958(7)	0	1.0
$Cr_{0.34}Re_{0.66}O_2$					
Re/Cr	$2a$	0	0	0	0.66/0.34
O	$4f$	0.2946(9)	0.2946(9)	0	1.0

Table 3
Selected interatomic distances (Å) and angles (deg) for three different $Cr_xRe_{1-x}O_2$ compositions from single crystal analysis, CrO_2 and ReO_2 from the literature.

Distances (Å) and angles (deg)	$Cr_{0.54}Re_{0.46}O_2$	$Cr_{0.50}Re_{0.50}O_2$	$Cr_{0.34}Re_{0.66}O_2$	CrO_2 [13]	ReO_2 [15]
Re/Cr–O	1.943(8) (× 2)	1.954(5) (× 2)	1.953(6) (× 2)	1.9048(5) (× 2)	1.973(1) (× 2)
Re/Cr–O	1.963(6) (× 4)	1.966(4) (× 4)	1.966(4) (× 4)	1.9008(3) (× 4)	1.998(1) (× 4)
Cr(Re)–Cr(Re)	2.914(2)	2.861(4)	2.836(3)	2.9154(1)	2.8091(1)
O–Re–O	95.8(4) (× 2)	93.4(2) (× 2)	92.3(3) (× 2)		

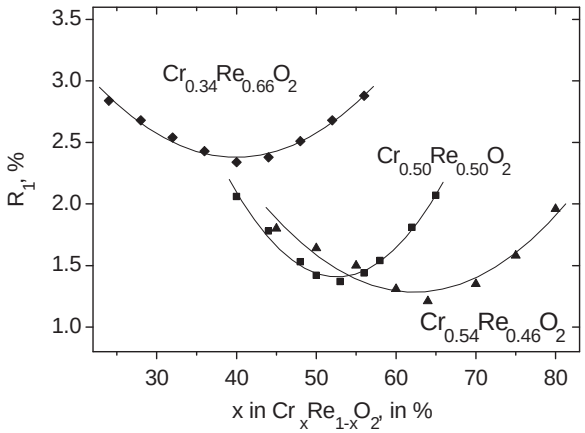

Fig. 3. R_1 values [$I>2\sigma(I)$] vs. Cr-content x, obtained by the refinement of the crystal structures of three $Cr_xRe_{1-x}O_2$ samples based on X-ray single crystal data. The specific Cr/Re ratios in the formula of these phases were obtained by EPMA.

see Fig. 3, due to the strong correlation with the corresponding thermal displacement parameters. Therefore, we have fixed the Cr/Re ratios during structure refinement as determined by EPMA. It correlates satisfactorily with the initial compositions.

3.2.2. *Crystal structure of $Cr_xRe_{1-x}O_2$ with cation order*

Structural parameters of tetragonal and monoclinic $Cr_xRe_{1-x}O_2$ were refined from X-ray powder diffraction data (Table 4). The crystal structure of the low-temperature form of $NiRe_2O_6$ [34] was chosen as the starting model for structural refinement of monoclinic $Cr_xRe_{1-x}O_2$. It crystallizes in $C2/m$ space group with different lattice parameters depending on x. For the compound with the refined "x"-values close to 0.500 Cr and Re are completely ordered on the (4i)- and (4g)-sites, respectively. The lattice parameters are $a=9.3482(2)$ Å, $b=5.6971(1)$ Å, $c=4.6121(1)$ Å, $\beta=91.995(1)^\circ$, and the metallic Re–Re distance is 2.579(2) Å. For the composition with the refined x-value of 0.459(4) the (4i)-site is occupied by both Cr and Re atoms, like by Ni and Re for monoclinic $NiRe_2O_6$, while the (4g)-site is exclusively occupied by Re ions with a corresponding Re–Re distance of 2.622(9) Å. This distance is shorter than in Re-metal (2.74 Å) and therefore interpreted as a metallic Re–Re bond. For $Cr_{0.459(4)}Re_{0.541(4)}O_2$ the lattice parameters are $a=9.3824(4)$ Å, $b=5.6903(2)$ Å, $c=4.6289(2)$ Å, $\beta=91.912(3)^\circ$.

For the refinement of the Cr_2ReO_6 structure, tetragonal Cr_2TeO_6 [7] was used as the starting model. Cr_2ReO_6 crystallizes in a tetragonal trirutile-structure, space group $P4_2/mnm$, with ordering of Cr on (4e)- and Re on (2a)-sites, respectively. The lattice parameters $a=4.5418(1)$ Å and $c=8.9173(4)$ Å are in agreement with those from [16].

3.3. *Thermal behavior of tetragonal $Cr_xRe_{1-x}O_2$ ($x=0.50$ and 0.34)*

The thermal stability of $Cr_{0.50}Re_{0.50}O_2$ and $Cr_{0.34}Re_{0.66}O_2$ was checked by combined DTA/TG and XRD investigations. Both compounds, obtained by HPHT synthesis, decompose into Cr_2O_3, Re (met) and Re_2O_7(g) in Ar-atmosphere. The thermal stability of $Cr_xRe_{1-x}O_2$ increases significantly with increasing Re-content in the sample: the decomposition temperature is 966 K for $Cr_{0.50}Re_{0.50}O_2$ and 1241 K for $Cr_{0.34}Re_{0.66}O_2$. This explains the partial decomposition of $Cr_xRe_{1-x}O_2$ with $x\geqslant 0.39$ during syntheses at $T>1023$ K in sealed silica tubes. Under the same conditions ReO_2 (Alfa Aesar, 99.99%) decomposes into Re(met.) and Re_2O_7(g) at 1227 K.

The high-temperature structural behavior of $Cr_{0.50}Re_{0.50}O_2$ and $Cr_{0.34}Re_{0.66}O_2$ samples was investigated in the temperature range of 295–1173 K by means of X-ray synchrotron diffraction. No phase transition was found for both phases. The temperature dependences of relative changes of the lattice parameters, normalized to their values at 295 K, are shown in Fig. 4. For $Cr_{0.34}Re_{0.66}O_2$ the "a" and "c" parameters increase linearly with temperature in the range from 295 to 1173 K, whereas for $Cr_{0.50}Re_{0.50}O_2$ the "a" parameter becomes smaller and "c" larger at $T>800$ K, which can be caused by a partial evaporation of Re in form of Re_2O_7(g) and therefore a change of the composition of the solid phase. The lattice parameters of "$Cr_{0.50}Re_{0.50}O_2$" after this high-temperature treatment correspond to a phase with higher Cr-content and confirm this proposed explanation.

Table 4
Structure parameters for the tetragonal and monoclinic Cr,Re-oxides, obtained by HPHT-synthesis.

Phase	Cr_2ReO_6	$CrReO_4$
Space group	$P4_2/mnm$	$C2/m$
a (Å)	4.5420(1)	9.3483(2)
b (Å)	4.5420(1)	5.6971(1)
c (Å)	8.9173(4)	4.6121(1)
β (deg)	90	91.99(1)
V (Å^3)	183.96(1)	245.48(1)
Z	2	8
Cr	4e	4i
X	0	0.2530(9)
Y	0	0
Z	0.3329(8)	0.5050(19)
Re	2a	4g
X	0	0
Y	0	0.7737(2)
Z	0	0
O(1)	4f	8j
X	0.2930(18)	0.1483(4)
Y	0.2930(18)	0.2303(11)
Z	0	0.2933(9)
O(2)	8j	4i
X	0.2985(12)	0.1249(9)
Y	0.2985(12)	0
Z	0.3383(12)	0.7820(20)
O(3)		4i
X		0.4104(9)
Y		0
Z		0.2450(20)
D(Cr–O) (Å)	1.972(8)	1.916(9)
D(Re–O) (Å)	1.919(9)	2.016(6)
Bragg R-factor (%)	2.85	3.44
R_F-factor (%)	2.18	2.66

The thermal expansion of tetragonal $Cr_xRe_{1-x}O_2$ is highly anisotropic. The average coefficient of expansion along the "*c*" axis is about ten times higher than along the "*a*" axis (Table 5). A similar but less pronounced anisotropy was observed for simple oxides adopting the rutile-structure, for example for TiO_2 ($\alpha_a = 7.3\times10^{-6}\,K^{-1}$ and $\alpha_c = 8.9\times10^{-6}\,K^{-1}$) or for VO_2 ($\alpha_a = 5.3\times10^{-6}\,K^{-1}$ and $\alpha_c = 27.5\times10^{-6}\,K^{-1}$) [30]. The anisotropy becomes more pronounced with increasing number of *d*-electrons from Ti, V to (Cr,Re) and might reflect electronic correlations, although no metal–metal bounds were found in these systems with tetragonal rutile-type structure.

3.4. Magnetic properties

The members of the tetragonal $Cr_xRe_{1-x}O_2$ solid solution show a Curie–Weiss behavior in the temperature range of 50–350 K with a maximum of magnetization below 50 K depending on composition *x* (Table 6). For $Cr_{0.54}Re_{0.46}O_2$, a spontaneous magnetization was observed at least up to 350 K, as example *M*(*H*) at 90 K in Fig. 5(a), but the detailed analysis of magnetization vs. temperature at different fields proofs unambiguously the presence of a (yet unknown) ferromagnetic phase in minimal quantity and the paramagnetic behavior of

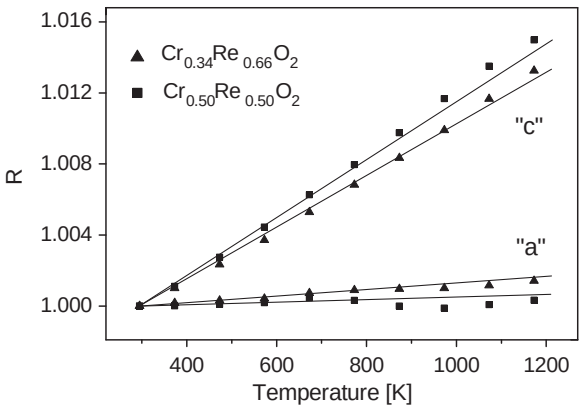

Fig. 4. Relative changes of lattice parameters $R = (a_T - a_{295\,K})/a_{295\,K}$ for $Cr_{0.34}Re_{0.66}O_2$ (triangles) and $Cr_{0.50}Re_{0.50}O_2$ (squares), normalized to their 295 K values. Note that the observed values at high temperature are larger than the linear extrapolation for the "*c*"-parameters and lower for the "*a*"-parameters.

Table 5
Average linear coefficients of thermal expansion of $Cr_{0.50}Re_{0.50}O_2$ and $Cr_{0.34}Re_{0.66}O_2$.

Composition	$\alpha_a \times 10^6$ (K^{-1})	$\alpha_c \times 10^6$ (K^{-1})	Temperature range (K)
$Cr_{0.50}Re_{0.50}O_2$	0.9(2)	16.8(3)	295–800
$Cr_{0.34}Re_{0.66}O_2$	1.53(8)	15.2(2)	295–1173

$Cr_{0.54}Re_{0.46}O_2$ at least above 80 K. The slopes $(\Delta M/\Delta H)_T$ in the high-field region and the spontaneous magnetisations M_{sp}, determined as the extrapolated magnetisation to zero field, are given in Table 7 for different temperatures. The slopes are approximations for the magnetic susceptibilities and in agreement with a Curie–Weiss behavior above the local maximum at 43(1) K. By assuming that all Cr- and Re-ions contribute to the average paramagnetic moment (in fact only some of them do, because some of them belong to the ferromagnetic phase) and taking into account that the high-field slope underestimates the slope at low fields, a lower limit for the paramagnetic moment per cation of $1.96(1)\mu_B$ is obtained without a χ_0 contribution in Eq. (1) and of $1.74(4)\mu_B$ with such a temperature independent part. The very smooth decrease of M_{sp} with temperature indicates the presence of a ferromagnetic contribution with a T_C above 350 K.

The presence of an unknown second phase in the $Cr_{0.54}Re_{0.46}O_2$ sample was also detected by X-ray diffraction independently and confirms the interpretation that the magnetic properties result from two very different contributions. The finite slopes in *M*(*H*) at high fields for all temperatures indicate that the ferromagnetic components belong only to a small fraction of the sample and that the alignment of the magnetic moments has not reach saturation at $\pm 6T$.

For $Cr_{0.52}Re_{0.48}O_2$ a slight divergence between FC and ZFC-mode below 20 K was also detected, which could be also due to a presence of a very small amount of an unknown phase invisible by X-ray diffraction. The field dependence of magnetization did not show any hysteresis loop (see inset in Fig. 5(b)).

The temperature dependence of the inverse specific susceptibility χ_m^{-1} of $Cr_xRe_{1-x}O_2$ ($x = 0.34$, 050 and 0.52) is shown in Fig. 6. Magnetic moments μ_{eff}(exp) per formula unit $Cr_xRe_{1-x}O_2$ ($x = 0.31$, 0.34, 0.50, 0.52) are calculated from the Curie constant in the paramagnetic region, obtained from fitting Eq. (1) to the observed data (Table 6). The antiferromagnetic interactions become stronger with increasing Cr content as reflected by the higher Nèel temperatures T_N, approximated by the values of $T_{\chi max}$, and the more negative Curie–Weiss temperatures θ, accompanied by an increasing temperature independent contribution χ_0. The paramagnetic contribution in $Cr_{0.54}Re_{0.46}O_2$ fits excellent into this trend.

$$\chi(T) = \frac{C}{T-\theta} + \chi_0 \qquad (1)$$

Effective paramagnetic moments, μ_{eff}(cal), were calculated based on the simple ionic model with Cr^{+3} and Re ions in oxidation states between +6 and +4, and by taking just the spin-only contribution from Cr^{3+} into account: $\mu_{eff}(cal) = g\sqrt{S(S+1)x}$, where $g = 2$, $S = 3/2$ and x is the Cr content in the compound. The measured paramagnetic moments for $Cr_xRe_{1-x}O_2$ are much smaller than the calculated effective ones (Table 6), indicating an electronic configuration, different from the above described model. This is in contrast to $Cr_xMo_{1-x}O_2$, where a good

Table 6
Magnetic properties of $Cr_xRe_{1-x}O_2$ together with calculated (see text) values of μ_{eff}(cal).

Compound	$T_{\chi max}$ (K)	$\chi_0 \times 10^5$ (emu/g)	θ (K)	μ_{eff}(exp), μ_B	Temperature range for fit (K)	μ_{eff}(cal), μ_B
$Cr_{0.54}Re_{0.46}O_2$	43(1)	1.3(2)	−76(5)	⩾1.74(4)	80–300	2.85
$Cr_{0.52}Re_{0.48}O_2$	40.0(5)	1.02(5)	−34.3(1.5)	1.27(2)	40–350	2.79
$Cr_{0.50}Re_{0.50}O_2$	35.0(5)	0.48(2)	−40.5(2.1)	1.33(2)	40–350	2.74
$Cr_{0.34}Re_{0.66}O_2$	25.0(5)	0.37(1)	−23.5(9)	1.45(1)	40–345	2.26
$Cr_{0.31}Re_{0.69}O_2$	10(1)	0.17(2)	−13.9(8)	1.37(2)	15–350	2.16

The standard deviations in brackets are determined as the limits, for which an up to 10% higher residual is obtained in the least-square fit than for the optimum fit for Eq. (1). The analysis of the magnetic properties for the $x = 0.54$ sample is explained in the text.

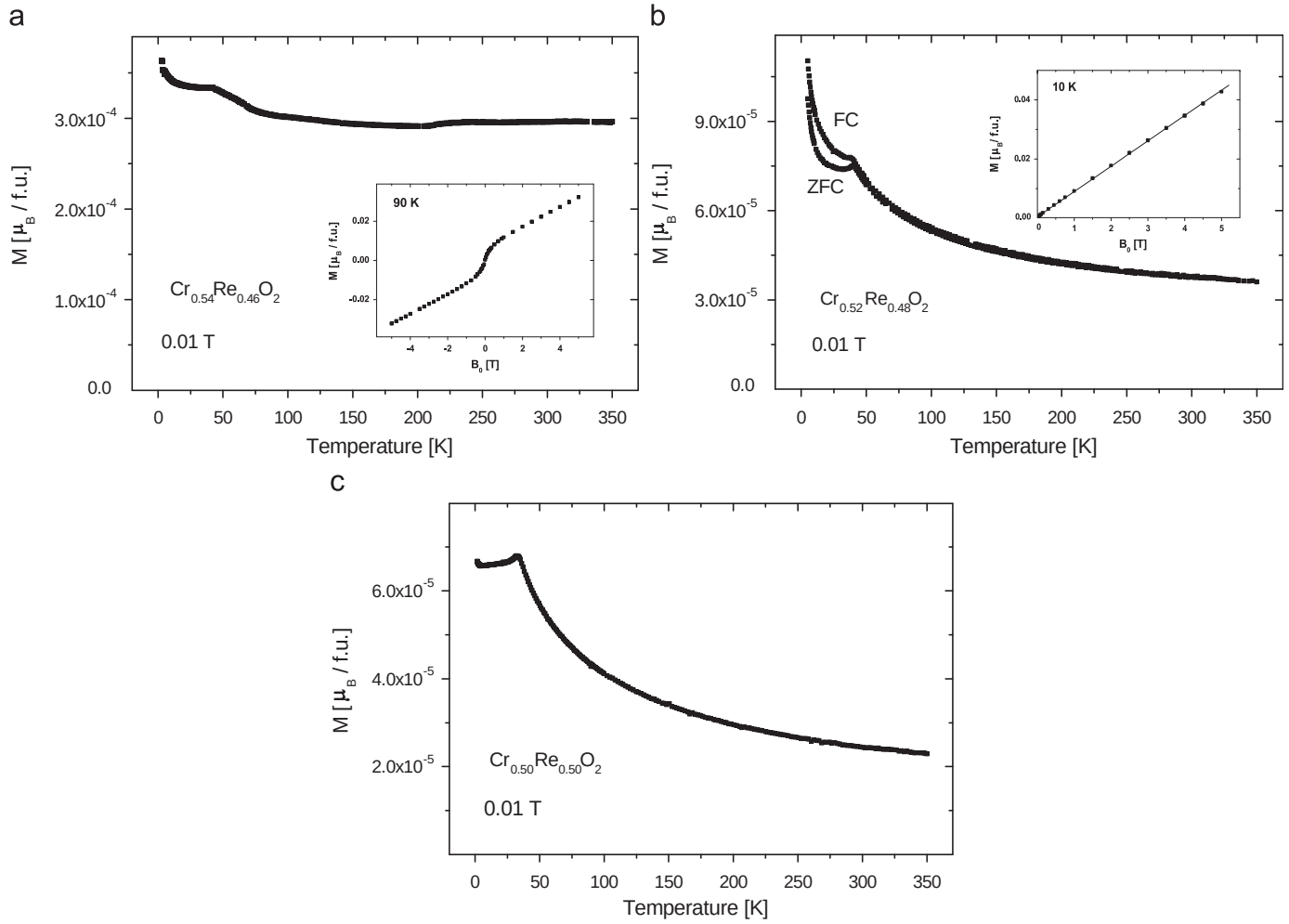

Fig. 5. Temperature dependence of the magnetic susceptibility for: (a) $Cr_{0.54}Re_{0.46}O_2$, (b) $Cr_{0.52}Re_{0.48}O_2$ with a field dependence of magnetization as an inset, and (c) $Cr_{0.50}Re_{0.50}O_2$. The inset in (a) shows the data of one representative field scan, used to separate the ferromagnetic component from the paramagnetic one.

Table 7
Separation of the measured magnetisations for $Cr_{0.54}Re_{0.46}O_2$ into a paramagnetic and a ferromagnetic contribution.

T (K)	$\Delta M/\Delta H$ (10^{-6} emu/g)	$M_{sp}(H\rightarrow 0)$ (10^{-3} emu)
5	0.181	0.519
80	0.160	0.435
100	0.145	0.431
110	0.135	0.428
125	0.127	0.423
145	0.116	0.419
200	0.0961	0.410
300	0.0734	0.390

The sample mass was 7.8(1) mg.

agreement between μ_{eff}(exp) and μ_{eff}(cal) was observed for this simple approximation [12]. A partial transfer of electrons could be proposed to explain the lower magnetic moments: $Cr^{+3}+Re^{+6} \Rightarrow Cr^{+4}+Re^{+5}$ and $Cr^{+3}+Re^{+5} \Rightarrow Cr^{+4}+Re^{+4}$. However, an intermediate state with a delocalisation of some electrons is more probable and should be reflected in the electronic structure.

3.5. Electronic structures

A metallic behavior can be concluded from a non-zero density of states at the Fermi edge E_F. The XPS valence spectra are shown in Fig. 7 for tetragonal $Cr_{0.5}Re_{0.5}O_2$ and a sample with overall composition "$Cr_{0.67}Re_{0.33}O_2$", containing tetragonal Cr_2ReO_6, monoclinic $Cr_{0.5}Re_{0.5}O_2$ and Cr_2O_3. For both samples the measured electron densities near E_F are not zero, so that both samples should show metallic behavior. The shape of the valence peaks is similar for the different $Cr_xRe_{1-x}O_2$ modifications,

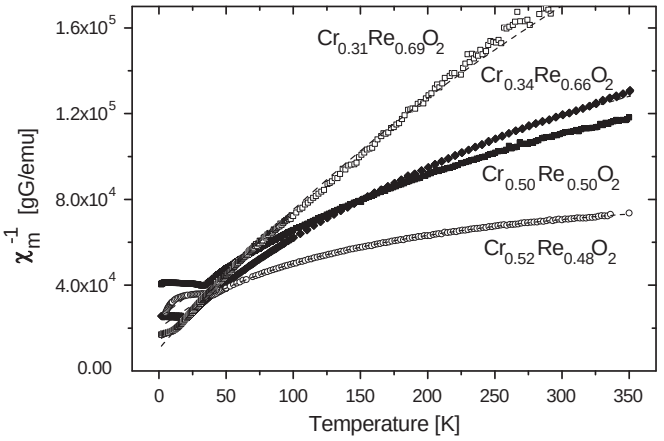

Fig. 6. Temperature dependence of the inverse specific magnetic susceptibility for $Cr_{0.52}Re_{0.48}O_2$, $Cr_{0.50}Re_{0.50}O_2$, $Cr_{0.34}Re_{0.66}O_2$ and $Cr_{0.31}Re_{0.69}O_2$.

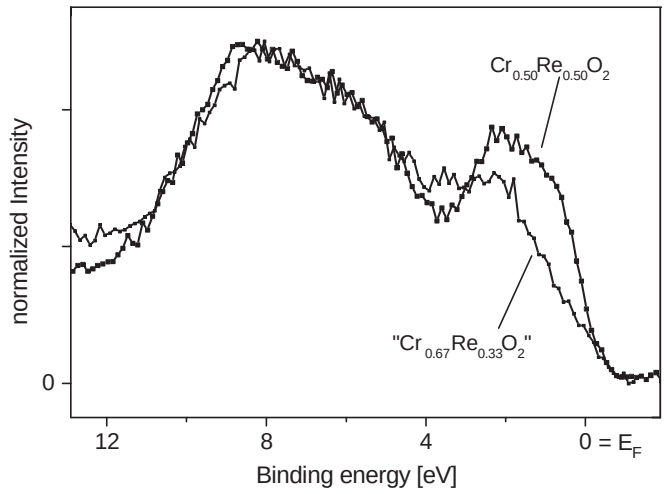

Fig. 7. XPS valence spectra of tetragonal $Cr_{0.5}Re_{0.5}O_2$ and "$Cr_{0.67}Re_{0.33}O_2$", containing monoclinic $Cr_{0.5}Re_{0.5}O_2$, tetragonal Cr_2ReO_6 and Cr_2O_3.

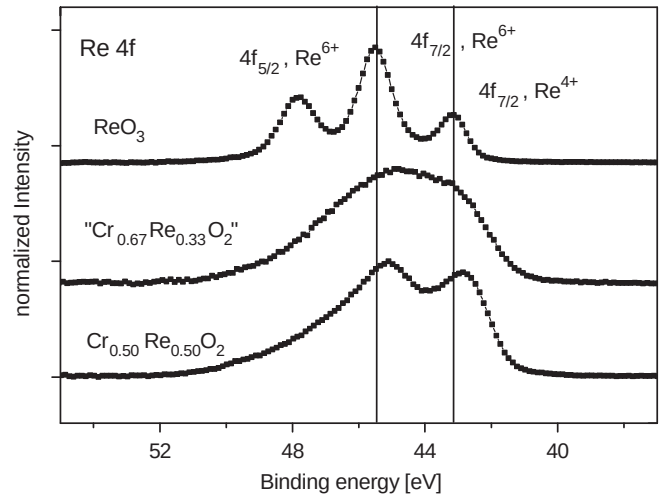

Fig. 8. Re4$f_{7/2}$ and 4$f_{5/2}$ core peaks of ReO_3 as a reference material, "$Cr_{0.67}Re_{0.33}O_2$", containing monoclinic $Cr_{0.5}Re_{0.5}O_2$, tetragonal Cr_2ReO_6 and Cr_2O_3, and phase-pure tetragonal $Cr_{0.5}Re_{0.5}O_2$.

resulting from the generic rutile-type structure. The small amounts of additional phases contribute only very weak signals, which are in good approximation proportional to their relative amounts and should not be critical for this interpretation, especially as Cr_2O_3 is an insulator. Although the XPS method represents an electronic structure of the surface region only and is influenced by contaminations or surface effects, the coexistence of Re ions in different oxidation states in oxides can be seen as a significant shift of the Re4$f_{7/2}$ core peaks [35]. Accordingly, we have previously established by XPS the presence of Re^{+4} and Re^{+6} in $CoRe_2O_6$ and $NiRe_2O_6$ with rutile-like structures, qualitatively confirmed by crystal structure analyses and magnetic measurements [34]. The Re4f peaks of $Cr_{0.5}Re_{0.5}O_2$ and "$Cr_{0.67}Re_{0.33}O_2$" are much broader in comparison to those of a ReO_3 reference material (Fig. 8). Note that the presence of the Re4$f_{7/2}$ peak of ReO_2 character at 43.6 eV in ReO_3 is due to a partial reduction in the surface-near region. The Re4f peak positions for the investigated Cr,Re-oxides correspond to oxidation states of Re between +4 and +6, and their broadening together with the finite density of states at E_F indicates a delocalisation of some electrons as expected from the magnetic behavior.

4. Discussion

A solid solution of $Cr_xRe_{1-x}O_2$ with tetragonal rutile-type structure and a random cation distribution on one site exists most probably only over a restricted composition range based on two observations: Firstly, for Cr_2ReO_6 ($Cr_{0.67}Re_{0.33}O_2$, $x = 0.67$) a trirutile structure with distinct Cr and Re sites is observed. Secondly, there is a pronounced non-monotonous behavior and discontinuity in the "a" vs. "c" dependence for all $Cr_xRe_{1-x}O_2$ compounds with respect to the end member CrO_2, see Fig. 9, which includes also samples with some but small enough impurities to allow a reliable estimate of the composition of the main phase. A broad and comprehensive homogeneity range for all compositions with a smooth evolution of structures and properties would be accompanied by a linear dependence of "a" and "c" parameters on composition, scaling with the cationic radii as observed for example for $CrSb_xV_{1-x}O_4$ [4]. Fig. 10 shows the dependence of "a" and "c" lattice parameters on Cr-content x in $Cr_xRe_{1-x}O_2$ together with the tetragonal modification of ReO_2 [15] and CrO_2 [13] as the end members and Cr_2ReO_6 with trirutile structure. Both dependences are fitted by exponential functions in the composition region from $x = 0$ (ReO_2) to $x = 0.67$ (Cr_2ReO_6) and these fits are shown as guides for the eyes in Fig. 10. With the increase of Cr content in $Cr_xRe_{1-x}O_2$ the average cationic radius decreases with the assumption of Cr^{3+} over the whole

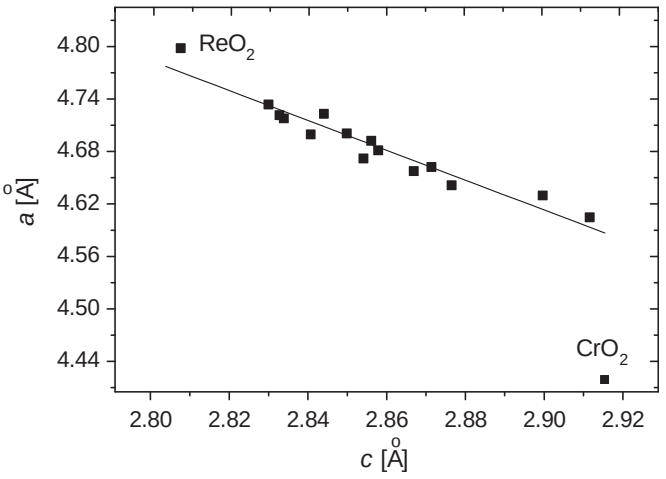

Fig. 9. The dependence of "a" parameter vs. "c" for $Cr_xRe_{1-x}O_2$, including the tetragonal modification of ReO_2 [15] and CrO_2 [13].

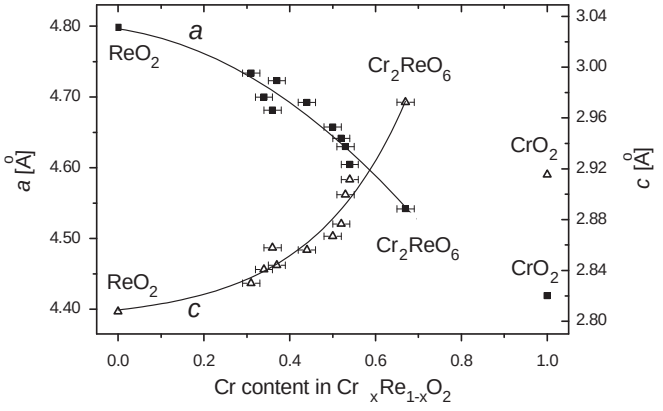

Fig. 10. Lattice parameters "a" and "c" vs. Re-content in $Cr_xRe_{1-x}O_2$. Lattice parameters for CrO_2 and ReO_2 (tetr.) are taken from [13,15]. For comparison $c/3$ is plotted for the trirutile structure with an otherwise three-fold c parameter due to the cation order.

composition range and a coexistence of Re^{+5} and Re^{+4} for $x<0.5$, Re^{+5} for $x=0.5$ and Re^{+5} and Re^{+6} for $x>0.5$: $r(Re^{+6})=0.55$ Å, $r(Re^{+5})=0.58$ Å and $r(Re^{+4})=0.63$ Å [3]. Therefore, a decrease of lattice parameters could be expected. The evolution of "*a*" is in agreement with this hypothesis. The same behavior of the "*a*" parameter along the replacement of a larger ion by a smaller one is reported for a lot of other related solid solutions with rutile-type structures, for instance, $Cr_xMo_{1-x}O_2$ ($0.0<x<0.5$) [12], $CrSb_xV_{1-x}O_4$ ($0.0\leqslant x\leqslant 1.0$) [4], $Nb_xCr_{1-x}O_2$ ($0.0\leqslant x\leqslant 0.9$) [26] or $Ti_{1-x}Cu_{x/3}Nb_{2x/3}O_2$ ($0.0\leqslant x\leqslant 0.9$) [27]. In the case of the $Cr_xMo_{1-x}O_2$ solid solution unit cell parameters for the whole range $0.0<x<0.5$ were calculated on the basis of a tetragonal rutile cell using appropriate transformation [11]. In contrast to the smaller average ionic radius the "*c*"-parameter in $Cr_xRe_{1-x}O_2$ becomes larger. The average Re oxidation state increases non-linear with the increasing of Cr^{3+} content in $Cr_xRe_{1-x}O_2$ (from 4 at $x=0$ and 5 at $x=0.5$ to 6 at $x=0.67$). As a result, there are less electrons available for the formation of a Re–Re metallic bond, which could be formed along c-axis and must cause its contraction. The increase of the average Re valence could therefore explain the increase of "*c*" with Cr content in the solid solution. The same tendency was found for other complex oxides with rutile-like structures. A strong intermetallic bonding and a decrease of *c*-axis was detected for $V_xMo_{1-x}O_2$ (d^1-configuration of V^{+4}, d^2-configuration of Mo^{+4}) at the replacement of smaller V^{+4} by larger Mo^{4+} [29], whereas no metal–metal bonding and an increase of the "*c*" parameter was observed for $V_xTi_{1-x}O_2$ (d^1-configuration of V^{+4}) at the replacement of smaller V^{4+} by larger Ti^{+4} [28]. In the case of the $Cr_xRe_{1-x}O_2$ solid solution metallic Re–Re bonds can be induced by the application of pressure during synthesis, accompanied by an underlying monoclinc structure with cation order.

For $Cr_{0.54}Re_{0.46}O_2$, the presence of a small amount of an unknown phase was observed, which has similar ferromagnetic properties as CrO_2. However, the unknown phase has much lower coercivity than CrO_2, and the formation of CrO_2 can be excluded for the specific conditions of synthesis. For CrO_2, the authors of [31] have shown by band structure calculations (LSDA+U) that, due to the slight distortion of the CrO_6 octahedra (two longer and four shorter Cr–O bonds) and the type of their connectivity in the structure, the *d*-bands of Cr are split into two parts: a localized band below the Fermi level having almost pure *d* character and filled with spin-down electrons, and highly dispersive and strongly hybridized *d*-bands, filled with spin-up electrons and crossing the Fermi level. In the latter case relative strong covalent interactions between *d* electrons of Cr and *p* electrons of O occur. Above T_c, a lower measured paramagnetic moment of Cr^{+4} compared with the theoretically calculated one was registered for CrO_2 [32]. According to our structural data, $Cr_xRe_{1-x}O_2$ phases do not show this kind of distortion of MO_6 octahedra, but rather the one of ReO_2 [15]: two shorter and four longer *M*–O distances (Table 3). The ground state of rutile-like ReO_2 ($5d^3$ configuration of Re^{+4}) is an AFM metal with a magnetic moment of $1\mu_B$ according to band structure calculations in the LDA+U approximations [15]. The lowest band has predominantly O 2*p* character, whereas the band crossing the Fermi level is occupied by a majority of Re 5*d* states. A strong covalent bonding between O and Re atoms was predicted [15] for both bands. $Cr_xRe_{1-x}O_2$ phases with $x<0.52$ order antiferromagnetically as calculated for ReO_2 with the rutile-structure. The very small paramagnetic moments per ion indicate that some electrons of Re and Cr in $Cr_xRe_{1-x}O_2$ are involved in metallic bonds or delocalized, resulting in a metallic conductivity. Such a scenario can also explain the increase of χ_0 with Cr content as a result of more Pauli paramagnetic contributions. In order to determine the character of conductivity and the number of conducting electrons, larger single crystals of $Cr_xRe_{1-x}O_2$ than available now would be required. Band structure calculations are essential to reveal the electronic structure of rutile-like $Cr_xRe_{1-x}O_2$ for different Cr-contents *x*. This would elucidate the role of changes from localized to delocalized electrons, maybe with intermediate metallic Re–Re bonds, for the transition from an antiferromagnetic to a ferromagnetic ground state.

Acknowledgments

The authors are indebted to C. Fasel (Institute for Materials Science, Darmstadt University of Technology, Germany) for performing the DTA measurements, B. Thybusch (Institute for Materials Science, Darmstadt University of Technology, Germany) for performing the EPMA measurements, and S. Leipe (Max-Planck Institute for Chemical Physics of Solids, Dresden, Germany) for performing the HPHT preparations in a multianvil press. Financial support from the *Bundesministerium für Bildung und Forschung* under Grant no. 05KSO7D2 is gratefully acknowledged.

References

[1] A.W. Wells, Structural Inorganic Chemistry, fifth ed., Clarendon Press, Oxford, 1984.
[2] W.H. Baur, Crystallogr. Rev. 13 (2007) 65–113.
[3] R.D. Shannon, Acta Crystallogr. A 32 (1976) 751–767.
[4] T. Tojo, Q. Zhang, F. Saito, J. Solid State Chem. 179 (2006) 433–437.
[5] K. Kristian, K.D. Singh Mudher, G.A. Rama Rao, V. Venugopal, J. Alloys Compd. 316 (2001) 264–268.
[6] V.K. Trunov, L.M. Kovba, Izvestiya Akademii Nauk SSSR, Neorganicheskie Materialy 2 (1966) 151–154.
[7] W. Kunnmann, S.J. la Placa, L.M. Corliss, J.M. Hastings, E. Banks, J. Phys. Chem. Solids 29 (1968) 1359–1364.
[8] A. Collomb, J.J. Capponi, M. Gondrand, J.C. Joubert, J. Solid State Chem. 23 (1978) 315–319.
[9] C. Gleitzer, J. Less Common Met. 51 (1977) 215–224.
[10] J.-P. Doumerc, S. Angelov, F. Ménil, M. Pouchard, Mat. Res. Bull. 11 (1976) 673–680.
[11] A. Sundholm, S. Andersson, A. Magnéli, B.-O. Marinder, Acta Chem. Scand. 12 (1958) 1343–1344.
[12] Y. Shimony, L. Ben-Dor, Mater. Res. Bull. 15 (1980) 227–232.
[13] P. Porta, M. Marezio, J.P. Remika, P.D. Dernier, Mater. Res. Bull. 7 (1972) 157–162.
[14] H.P.S. Correa, I.P. Cavalcante, L.G. Martinez, C.G.P. Orlando, M.T.D. Orlando, Braz. J. Phys. 34 (2004) 1208–1210.
[15] A.L. Ivanovskii, T.I. Chupakhina, V.G. Zubkov, A.P. Tyutyunnik, V.N. Krasilnikov, G.V. Bazuev, S.V. Okatov, A.I. Lichtenstein, Phys. Lett. A 348 (2005) 66–70.
[16] A.W. Sleight, J. Solid State Chem. 14 (1975) 597–598.
[17] L. Zaitseva, Russ. J. Inorg. Chem. (Engl. Transl.) 24 (1979) 666.
[18] A. Butz, I. Svoboda, H. Paulus, H. Fuess, J. Solid State Chem. 115 (1995) 255–259.
[19] T. Roisnel, J. Rodriguez-Carvajal, Mater. Sci. Forum 378–381 (2001) 118–123.
[20] G.M. Sheldrick, Acta Crystallogr. A 46 (1990) 467–473.
[21] G.M. Sheldrick, SHELXL97, Program for the Refinement of Crystal Structures, University of Göttingen, Germany, 1997.
[22] Stoe & Cie, X-STEP32, Stoe & Cie GmbH, Darmstadt, Germany, 2000.
[23] M. Knapp, C. Baehtz, H. Ehrenberg, H. Fuess, J. Synchrotron Radiat. 11 (2004) 328–334.
[24] M. Knapp, V. Joco, C. Baehtz, H.H. Brecht, A. Berghaeuser, H. Ehrenberg, H. von Seggern, H. Fuess, Nucl. Instrum. Methods A 521 (2004) 565–570.
[25] W.H. Baur, W. Joswig, G. Pieper, D. Kassner, J. Solid State Chem. 99 (1992) 207–211.
[26] Y. Shimony, L. Ben-Dor, J. Mater. Sci. Lett. 2 (1983) 558–560.
[27] A. Grandin, M.M. Borel, C. Michel, B. Raveau, Mater. Res. Bull. 18 (1983) 239–246.
[28] B.-O. Marinder, A. Magneli, Acta Chem. Scand. 11 (1957) 1635–1640.
[29] B.-O. Marinder, Mater. Res. Bull. 10 (1975) 909–914.
[30] L.G. Van Uitert, H.M. O'Bryan, H.J. Guggenheim, R.L. Barns, G. Zydzik, Mater. Res. Bull. 12 (1977) 307–314.
[31] M.A. Korotin, V.I. Anisimov, D.I. Khomskii, G.A. Sawatzky, Phys. Rev. Lett. 80 (1998) 4305–4308.
[32] B. Chamberland, CRC Crit. Rev. Solid State Mater. Sci. 7 (1977) 1.
[33] A. Magneli, Acta Chem. Scand. 11 (1957) 28.
[34] D. Mikhailova, H. Ehrenberg, S. Oswald, D. Trots, G. Brey, H. Fuess, J. Solid State Chem. 182 (2009) 364–373.
[35] J.F. Moulder, W.F. Stickle, P.E. Sobol, K.D. Bomben, Handbook of X-ray Photoelectron Spectroscopy, Physical Electronics, Inc., 1995.